Available online at website: https://journal.bcrec.id/index.php/bcrec

Bulletin of Chemical Reaction Engineering & Catalysis, 21 (1) 2026, 226-243

Original Research Article

Bimetallic Ni–Cu/ZSM-5 Catalysts for Enhanced Phenol and Vanillin Production from Benzyl Phenyl Ether and Lignin

Arnia Putri Pratama[1,2], Iman Abdullah[1,2], Yuni Krisyuningsih Krisnandi[1,2*]

[1]Department of Chemistry, Faculty of Mathematics and Natural Sciences, Universitas Indonesia, Kampus UI Depok, Depok 16424, Indonesia
[2]Solid Inorganic Framework Laboratory, Department of Chemistry, Faculty of Mathematics and Natural Sciences, Universitas Indonesia, Kampus UI Depok, Depok 16424, Indonesia.

Received: 12th December 2025; Revised: 14th January 2026; Accepted: 15th January 2026
Available online: 18th January 2026; Published regularly: April 2026

Abstract

Bio-based phenolic chemicals from lignin represent a sustainable alternative to fossil aromatics. This study examines the catalytic conversion of benzyl phenyl ether (BPE) and compares its reactivity with isolated lignin from raw woody biomass waste (ILWB). Hierarchical ZSM-5 zeolite catalysts were synthesized and modified with bimetallic Ni–Cu and monometallic (Ni^0 and Cu^0) species. Catalyst characterization by Fourier Transform Infra-Red (FTIR), X-ray Diffraction (XRD), Scanning Electron Microscope - Energy Dispersive X-Ray (SEM-EDX), X-ray Fluorescence (XRF), and Brunauer, Emmett, and Teller (BET) surface area confirmed distinct physicochemical features for each catalyst. Catalytic reactions were conducted in a batch reactor at 100–300 °C for 30 minutes. Products were analyzed by HPLC, identifying phenol and vanillin as key products. The bimetallic Ni–Cu/ZSM-5 catalyst exhibited alloy formation, producing a synergistic effect that enhanced catalytic activity. BPE conversion reached 94.29%, with a phenol yield of 32.25% at 250 °C. Additionally, ILWB lignin was readily converted, achieving 75.31% conversion and a vanillin yield of 15.85% at 200 °C. These findings confirm that Ni–Cu-modified hierarchical ZSM-5 demonstrates superior catalytic behavior for the valorization of lignin and its model compound into high-value chemical products.

Keywords: Bimetallic Ni–Cu; Hierarchical ZSM-5; BPE; Lignin; Phenol; Vanillin

How to Cite: Pratama, A. P., Abdullah, I., Krisnandi, Y. K. (2026). Bimetallic Ni–Cu/ZSM-5 Catalysts for Enhanced Phenol and Vanillin Production from Benzyl Phenyl Ether and Lignin. *Bulletin of Chemical Reaction Engineering & Catalysis*, 21 (1), 226-243. (DOI: 10.9767/bcrec.20559)

Permalink/DOI: https://doi.org/10.9767/bcrec.20559

1. Introduction

Each year, the pulp and biorefinery industries generate approximately 50 to 70 million tons of lignin as waste from lignocellulosic processing [1,2]. However, over 98 percent of this lignin is merely combusted as low-calorific-value fuel [3], while less than 2 percent is utilized as a feedstock for high-value chemicals [4]. Lignin, a key constituent of lignocellulosic biomass that represents the most abundant renewable resource on Earth, exists in more than 300 billion tons within the biosphere and contains approximately 15 to 30 percent of organic carbon [5]. With global biomass production exceeding 1.4 billion dry tons annually, the valorization of lignin as a precursor for renewable chemicals and fuels presents a promising opportunity to reduce industrial waste while promoting the transition toward a circular, bioenergy-based economy [6]. This effort is becoming increasingly critical in light of the limited availability of fossil resources and their substantial contribution to greenhouse gas emissions and the global climate crisis [7]. Therefore, the development of efficient and environmentally friendly strategies for lignin conversion plays an important role in achieving sustainability in energy and chemical production.

Bio-based resources constitute plentiful, carbon-rich, and renewable materials that can be

* Corresponding Author.
Email: yuni.krisnandi@sci.ui.ac.id (Y. K. Krisnandi)

converted through various chemical or biochemical pathways into high-value chemicals, sustainable fuels, and advanced biobased materials [8]. Among them, lignocellulosic biomass is particularly promising, consisting of lignin (±15-30%), cellulose (±35-50%), and hemicellulose (±20-35%) [9]. Lignin is a renewable aromatic polymer with high potential for conversion into valuable compounds, including phenol and vanillin, which are the primary target products in this study. Phenol is chosen due to its key role as a precursor for phenolic resins, engineering plastics, and various industrial intermediates, with an estimated global demand exceeding 15 million tons annually [10]. Vanillin is also considered a valuable compound, serving as a sustainable alternative to bisphenol A in bio-aromatic polymers due to its low toxicity and renewable origin [11] . Focusing on these two compounds emphasizes a selective and application-driven strategy for lignin valorization.

Phenolic aromatic compounds in bio-oils can be obtained from lignin derivatives through pyrolysis processes involving heterogeneous catalysts, such as $NiCl_2$/ZSM-5 [12], Co/HZSM-5 [13], Ni/Al_2O_3-SiO_2 [14], metal oxide (CuO, CeO_2, Mn_2O_3, NiO) [15]. These processes are typically carried out at temperatures ranging 400 ^oC – 700 ^oC for durations of 30 minutes to 4 hours, producing phenolic yields 0.06% - 30.2% with selectivity ranging 9.2% - 35%. In addition to conventional pyrolysis, fast pyrolysis using Mo/ZSM-5 [16] at 600 ^oC and Cu/HZSM-5 at 550 ^oC [17] has also shown potential. Alternatively, hydrogenolysis has emerged as a milder depolymerization route for lignin-derived compounds. For example, bimetallic Pd and Co catalysts can convert benzyl phenyl ether (BPE) at 240 ^oC for 180 minutes, resulting in 30% yield aromatics with 50%:50% selectivity toward phenol:toluene [18]. Yan *et al.* reported efficient depolymerization of organosolv lignin using Ni-Cu-Mo_2C/AC and optimum catalyst using Ni-Fe-Mo_2C/AC at 260 ^oC for 4 hours, achieving monomer yields ranging 25.12%-35.53% [19]. Other effective catalysts include Cu/ZSM-5 for protobind lignin depolymerization under 5 hours at 440 ^oC with monomer yields 98.2% including ~2% of 2-ethylphenol and ~10% of toluene [20] and efficient transfer hydrogenolysis of BPE under NiCu/Al_2O_3 catalysts resulting in 5.12-37.42% yield phenol at 200 ^oC during 2 hours [21]. On the other hand, Korányi *et al.* reported a hydrodeoxygenation (HDO) reaction of soda lignin that produced 9.1% - 15.4% aromatic yield with a total lignin monomer yield of 28% - 49% percent using CuMgAlOx + Ni/ASA and Ni/ASA (amorphous silica alumina) catalysts under conditions of 340 °C for 4 hours [22]. The HDO of BPE was also investigated using NiMo/γ-alumina-USY-zeolite and NiMo/USY-zeolite catalysts, resulting in greater than 99% BPE conversion at 320 °C for 6 hours, with 13% - 18% phenol yield and 44.5% - 59% yield of total deoxygenated aromatics (BTX) [23].

Inorganic framework materials based on zeolites, especially hierarchical ZSM-5, are frequently utilized as solid catalytic systems owing to their characteristic properties such as tunable acidity, high surface area, adjustable pore structure, and excellent thermal stability [24]. To enhance catalytic performance and selectivity toward target phenolic compounds from lignin conversion, ZSM-5 surfaces can be modified through the impregnation of transition metals such as nickel (Ni) and copper (Cu). Ni has been widely recognized for its effectiveness in cleaving C–O bonds in lignin model compounds, including BPE, via hydrogenolysis and dehydrogenation mechanisms [8], whereas Cu serves as a selectivity promoter by stabilizing aromatic intermediates and suppressing over-hydrogenation [21,25]. The Ni and Cu bimetallic system exhibits synergistic effects that enhance metal dispersion, improve thermal stability, and mitigate deactivation [21]. Accordingly, the integration of Ni and Cu into hierarchical ZSM-5 frameworks offers a promising catalytic approach for the efficient and sustainable conversion of lignin into phenolic fine chemicals.

Although zeolite-based catalysts have been extensively applied for biomass conversion, comprehensive studies investigating the role of bimetallic Ni-Cu on hierarchical ZSM-5 in enhancing selectivity toward phenolic products from lignin and model compounds such as benzyl phenyl ether (BPE) remain scarce. This research addresses this gap by evaluating the catalytic performance of hierarchical Ni–Cu/ZSM-5 during the thermal conversion of BPE without the use of external hydrogen. The study focuses on the impact of pore structure, metal dispersion, and surface acidity on BPE conversion and product selectivity toward phenol and vanillin. The results are expected to contribute to the development of advanced heterogeneous catalysts for the conversion of lignin into value-added chemicals, fine chemicals, and sustainable biofuels.

2. Materials and Methods

2.1. Materials

All chemicals utilized throughout this investigation possessed analytical-grade specifications: sodium aluminate ($NaAlO_2$, 99.0%), tetrapropylammonium hydroxide (TPAOH, 40.0%), tetraethyl orthosilicate (TEOS, 98.0%), polidialydimethyl ammonium chloride (PDDA-Cl, 35.0%), copper(II) nitrate trihydrate, nickel(II) nitrate hexahydrate, phenol and vanillin for synthesis were obtained from Sigma Aldrich. All reagents employed in this study were

of analytical-grade purity: ethanol (95.0%), methanol (95.0%), hydrogen peroxide (30.0%), phosphoric acid (89.0%), sodium hydroxide (99.0%), sulphuric acid (96.0%), were procured from Merck. All solutions were prepared using deionized water. The N_2 gases was supplied by CV. Retno Gas.

2.2. Catalyst Preparation

Hierarchical ZSM-5 zeolite was synthesized through a dual-template hydrothermal method, adapted from the procedure published in Helmi *et al*. [26]. In this synthesis, tetraethyl orthosilicate (TEOS) and sodium aluminate ($NaAlO_2$) served as the silicon and aluminum precursors, respectively. The synthesis gel was formulated according to molar ratios established in prior studies, comprising 0.29 g of $NaAlO_2$, 27.15 g of TEOS (98%), 25.94 g of TPAOH (40%), 111.83 mL of deionized water, and 1.0 g of PDDA-Cl. The mixture was thoroughly homogenized and transferred into a Teflon-lined stainless-steel autoclave (approximately 250 mL capacity). Tetrapropylammonium hydroxide (TPAOH) and poly(diallyldimethylammonium chloride) (PDDA-Cl) were used as the primary and secondary structure-directing agents, respectively. The hydrothermal crystallization was conducted at 170 °C for 6 days. Upon completion, the resulting white solid was filtered, washed, and calcined at 550 °C for 3 hours to remove organic templates, yielding a white hierarchical ZSM-5 powder.

The wet-impregnation procedure was adopted from Herlina *et al*. [25]. In contrast, the bimetallic design concept and the thermal treatment strategy for transforming metal species from M^{2+} to M^0 were inspired by Sofyani *et al*. [27].

The bimetallic Ni–Cu/hierarchical ZSM-5 catalyst was prepared by dissolving nickel nitrate hexahydrate ($Ni(NO_3)_2.6H_2O$) and copper nitrate trihydrate ($Cu(NO_3)_2.3H_2O$), which were dissolved to obtain a total metal loading of 10 wt% relative to the zeolite mass. The mixed-metal solution was then added to 1 g of hierarchical ZSM-5, and the mixture was stirred continuously at room temperature for 48 hours to form a uniform paste. The resulting paste was dried at 50–60 °C overnight, and subsequently thermally treated at 550 °C under a hydrogen flow in a tubular furnace to reduce the metal oxides (M^{2+}) into their metallic states (M^0), producing a grey Ni–Cu/ZSM-5 powder.

Monometallic Ni/ZSM-5 and Cu/ZSM-5 catalysts were prepared following a similar wet impregnation procedure. Each precursor, $Ni(NO_3)_2.6H_2O$ or $Cu(NO_3)_2.3H_2O$, was calculated to provide a 10 wt% metal loading with respect to 1 g of ZSM-5. The prepared solution was added dropwise to the zeolite and continuously stirred at room temperature for 48 hours to achieve a homogeneous paste. The obtained paste was dried overnight at 50–60 °C and calcined at 550 °C under hydrogen flow in a tubular furnace to produce hierarchical Ni/ZSM-5 and Cu/ZSM-5 catalysts in the form of light grey powders, respectively.

2.3. Characterization Techniques

The synthesized catalysts were examined through a series of analytical methods to elucidate their structural, textural, chemical, and acidity characteristics. X-ray Diffraction (XRD) measurements were performed on a PANalytical X'Pert PRO 2318 diffractometer operating with Cu-Kα radiation (λ = 1.54184 Å) as the incident beam, with a scanning range of 2θ = 5–50°, to confirm the crystalline structure and phase purity of the samples. The Si/Al ratio and metal content were determined by X-ray Fluorescence (XRF) analysis using an Orbis EDAX spectrometer operated at 100 kV and 40 mA. Fourier-transform infrared (FT-IR) spectra were obtained using an Alpha-Bruker spectrometer employing the KBr pellet technique (sample-to-KBr ratio of 1:20) under 128 scans in the wavenumber range of 4000–400 cm^{-1}, to identify the functional groups and verify the framework structure of the zeolite. The specific surface area, pore size distribution, and pore volume of the catalysts were analyzed using a Quantachrome Quadrasorb-Evo surface area and porosimetry instrument. The pore-size distribution was interpreted based on the Barrett–Joyner–Halenda (BJH) method applied to the desorption branch of the isotherms. The morphology and elemental distribution of the catalysts were examined using a JEOL JIB-4610F field-emission scanning electron microscope (SEM) coupled with an energy-dispersive X-ray spectroscopy (EDS) detector. The surface acidity was investigated through NH_3-temperature programmed desorption (NH_3-TPD) using a Micromeritics Chemisorb 2750 analyzer. Prior to NH_3 adsorption, 0.05 g of each catalyst sample was pretreated at 350 °C for 60 min under helium flow (inert atmosphere). The sample was then saturated with 5% NH_3 in He (v/v) at 100 °C for 30 min, purged with He gas at the same temperature for 30 min, and finally desorbed at 100–700 °C with a heating rate of 10 °C/min, held for 15 min at 700 °C, under a total flow rate of 40 mL/min.

2.4. Catalytic Activity Test

The catalytic reaction procedure was adapted from Ramadhani *et al.* [28], with minor modifications in the substrate selection. All catalytic reactions were carried out under an inert atmosphere by introducing nitrogen gas at 2 atm pressure at ambient temperature. A mixed solvent of water and ethanol (1:1, v/v) was used with a total volume of 12.5 mL. Two types of substrates

were employed in this study, namely benzyl phenyl ether (BPE) as a lignin model compound and isolated lignin from raw woody biomass waste (ILWB) as the real biomass substrate. The preparation procedure and yield calculation for ILWB followed our previously reported method [29]. The amount of substrate and catalyst used in each reaction was 0.125 g and 0.0625 g, respectively. The reactions were performed under continuous stirring at 300 rpm for 30 minutes, while the reaction temperature was varied at 100, 150, 200, 250, and 300 °C.

After completion of the reaction, the reaction mixture was filtered, and the resulting filtrate was collected for high-performance liquid chromatography (HPLC) analysis using a PG LC210 system fitted with a C18 analytical column. A mobile phase composed of methanol and distilled water (80:20, v/v) was used as the eluent. Product identification and quantification were performed by HPLC using authentic phenol and vanillin standards. Substrate conversion and the yields of phenol and vanillin were determined based on standard calibration curves and calculated according to the methods reported by Ramadhani *et al.* and Herlina *et al.* [28,30], using the following equations:

$$\%Substrate\ Conversion = \frac{Initial\ Substrate\ Mass\ (g) - Residual\ Mass\ (g)}{Substrate\ Mass\ (g)}\ x\ 100\% \quad (1)$$

$$\%Yield\ Product = \frac{Product\ Concentration\ (mg/L) - Solution\ Volume\ (L)}{Substrate\ Mass\ (mg)}\ x\ 100\% \quad (2)$$

3. Results and Discussion

3.1. Catalyst Characterizations

The X-ray diffraction (XRD) patterns of the synthesized hierarchical ZSM-5, monometallic Ni/ZSM-5 and Cu/ZSM-5, as well as the bimetallic Ni–Cu/ZSM-5 catalysts, are shown in Figure 1. All materials exhibited the characteristic reflections of the MFI-type zeolite framework within the 2θ ranges of 7–10° and 22–25°, corresponding to the (011), (020), (051), (303), and (313) planes of ZSM-5 [31]. These diffraction characteristics verify the successful formation of crystalline ZSM-5 with robust structural integrity. The presence of sharp, well-resolved reflections indicates that the pentasil framework remained intact throughout the synthesis procedure.

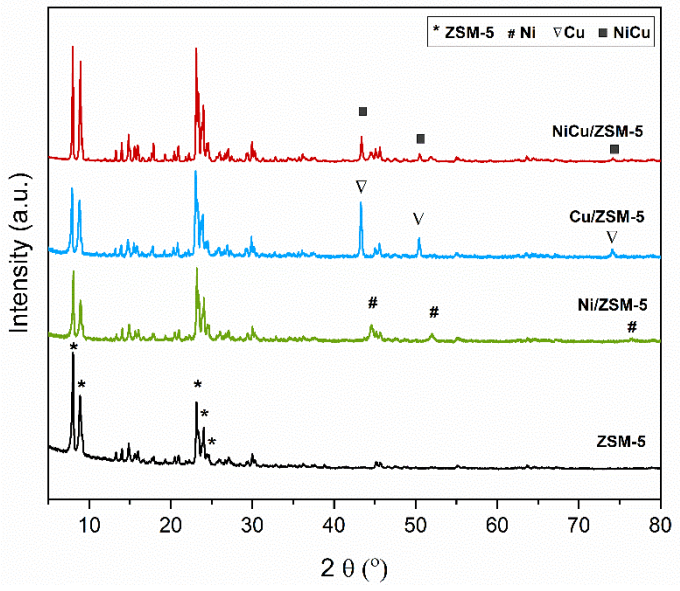

Figure 1. Powder XRD pattern of ZSM-5 catalysts.

After the impregnation of metallic Ni and Cu, the principal diffraction peaks of the ZSM-5 framework remained unchanged, indicating that the introduction of metal species did not distort or collapse the MFI structure. New reflections appeared in the metal-loaded catalysts, confirming the presence of metallic phases. Additional reflections emerged in the XRD profiles of the monometallic catalysts. For Ni/ZSM-5, new peaks appeared at 2θ = 44.56°, 51.95°, and 76.53°, corresponding to the (111), (200), and (220) planes of metallic Ni^0 (JCPDS 04-0850) [32]. Meanwhile, Cu/ZSM-5 showed distinct reflections at 43.26°, 50.45°, and 74.12°, assigned to metallic Cu^0 (JCPDS 04-0836) [33]. The absence of diffraction features associated with NiO or CuO suggests that the reduction treatment resulted in the predominant formation of metallic Ni and Cu species. Overall, these results confirm that the hierarchical ZSM-5 framework maintained its crystallinity and structural stability after metal deposition.

In the bimetallic Ni–Cu/ZSM-5 catalyst, distinct reflections were observed at 43.52°, 50.68°, and 74.51°, corresponding to the (111), (200), and (220) lattice planes of a Ni–Cu alloy phase (JCPDS 47–1406) [21]. These peak positions lie between the respective diffraction lines of metallic Ni^0 and Cu^0, demonstrating lattice integration that is characteristic of alloy formation. Owing to the close diffraction positions of Ni and Cu, partial overlap is expected; therefore, the subtle shifts detected around the (111) region further support the presence of a solid-solution Ni–Cu alloy rather than the simple coexistence of separate Ni and Cu domains. The alloy-associated reflections also appeared with greater definition than those of the monometallic samples, indicating enhanced crystallinity and a more uniform dispersion of the bimetallic particles. Although weak signals attributable to residual Ni^0 or Cu^0 phases were still detected, these minor peaks are commonly linked to small fractions of metal species that remain segregated on the zeolite surface due to differences in reducibility or local metal distribution. Overall, the XRD profile confirms successful alloy formation, with the Ni–Cu alloy

constituting the predominant metallic phase within the catalyst.

As supported by the XRD results, which confirm that the MFI framework remains intact after metal impregnation and reduction, the Fourier-transform infrared FTIR analysis provides additional evidence of structural preservation in ZSM-5 as shown in Figure 2. All samples exhibit the characteristic absorption bands of MFI-type zeolites at 1220 cm^{-1} (asymmetric T–O stretching), 1100–800 cm^{-1} (symmetric T–O stretching), and 550–500 cm^{-1}, verifying that metal modification does not disrupt the pentasil units of the framework [34]. The broad band at 3600–3200 cm^{-1} and the signal at 1630 cm^{-1} correspond to silanol groups and adsorbed water, respectively. The appearance of an organic-related band at 2974 cm^{-1} after metal introduction further indicates the successful incorporation of mono- and bimetallic species. Meanwhile, changes in the intensity of the silanol band among Ni–Cu/ZSM-5, Ni/ZSM-5, and Cu/ZSM-5 reflect surface interactions between Ni–Cu, Ni, and Cu species and the hydroxyl sites of the zeolite. Additionally, the enhanced symmetric stretching at 1101 cm^{-1} suggests stronger bonding interactions associated with the bimetallic Ni–Cu alloy.

Additional bands in the fingerprint region (1000–450 cm^{-1}) reveal subtle modifications arising from dispersed metal species, with the characteristic Ni bands appearing at approximately 453, 479, and 490 cm^{-1}, corresponding to Ni–O linkages and Ni–(OH) stretching vibrations [35]. Likewise, the characteristic Cu-related bands appear near 459, 477, and 494 cm^{-1}, associated with Cu–O and Cu–(OH) stretching [36]. The bimetallic Ni–Cu sample exhibits bands at around 460, 476, and 492 cm^{-1}. These variations are closely linked to modifications in the T–O–T environment caused by metal–silanol interactions and the possible formation of bimetallic active centers in Ni–Cu/ZSM-5, as indicated by intensity changes within the 550–450 cm^{-1} region. The detected absorption bands can also be associated with vibrational modes arising from Ni–O and Cu–O interactions. Collectively, the spectral characteristics elucidate the principal molecular features of the Ni–Cu system, offering insight into

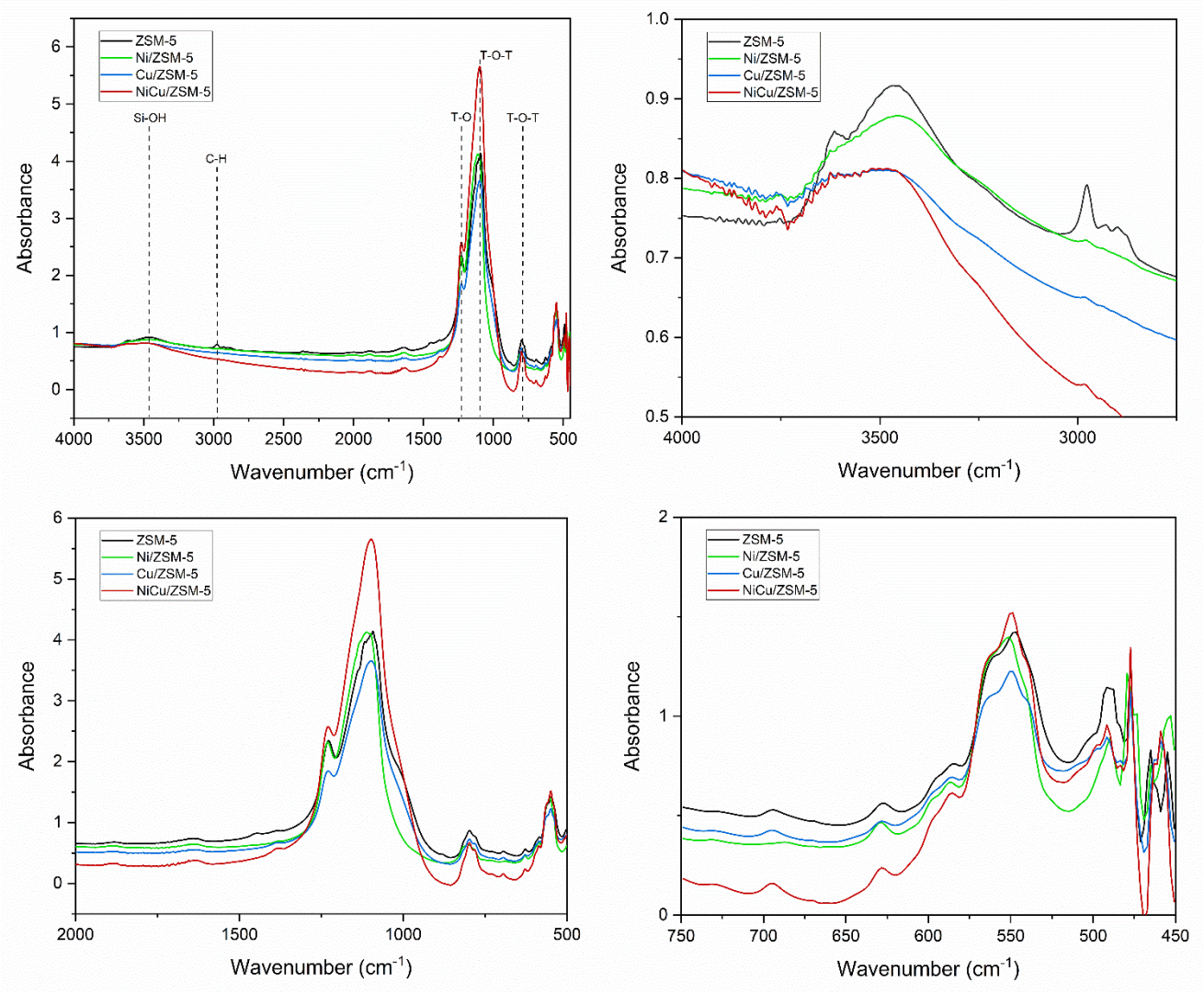

Figure 2. FTIR spectra of ZSM-5 catalysts.

the stretching and bending vibrations of functional groups and chemical bonds present within the material, particularly those manifested in the low-frequency region [37]. Accordingly, the FTIR data reinforces the conclusion that the impregnation and reduction steps successfully produced well-dispersed metal species on the ZSM-5 surface. This provides a structural foundation that supports the interpretation of the subsequent elemental, acidity, and catalytic activity characterizations.

The elemental composition of catalysts using X-ray fluorescence XRF and Energy Dispersive X-Ray Spectroscopy EDS analyses shows that the Si/Al ratios of all ZSM-5 samples remain stable after Ni, Cu, or NiCu impregnation, indicating that the metal modification process does not induce dealumination or structural changes within the zeolite framework. Based on the data summarized in Table 1, the Si/Al ratios show only minor variations before and after metal incorporation, confirming that the framework composition is largely preserved throughout the synthesis. The Ni and Cu loadings obtained by XRF closely match their theoretical values: 9.83 wt% Ni for Ni/ZSM-5, 10.04 wt% Cu for Cu/ZSM-5, and approximately 5 wt% of each metal for NiCu/ZSM-5. A comparable pattern is observed in the EDS results, further validating the successful deposition of the metal species. Slight discrepancies between XRF and EDS in the monometallic samples suggest that the metals are mainly enriched at the catalyst surface because EDS, which probes the outer layer, detects slightly higher metal levels than bulk-sensitive XRF [38]. Conversely, the close agreement between the two analytical methods in the bimetallic catalyst indicates a more uniform distribution of Ni and Cu throughout the material, consistent with enhanced Ni–Cu interactions that promote homogeneous metal dispersion.

As shown in Figure 3, the SEM analysis reveals that all catalysts, including ZSM-5, Ni/ZSM-5, Cu/ZSM-5, and the bimetallic Ni–

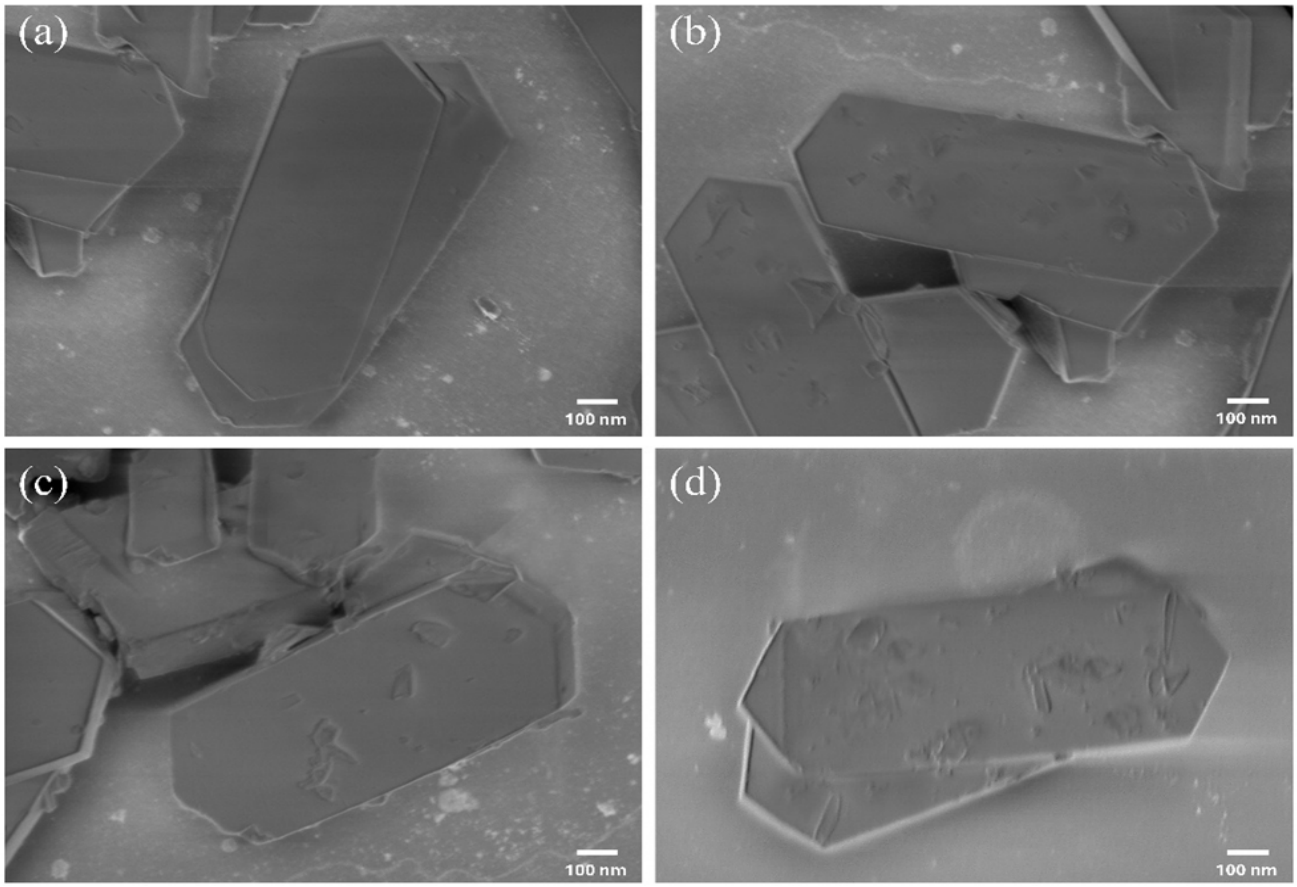

Figure 3. SEM images of (a) ZSM-5, (b) Ni/ZSM-5, (c) Cu/ZSM-5, and (d) NiCu/ZSM-5 catalysts.

Table 1. XRF and EDS analysis data (%wt) of ZSM-5, Ni/ZSM-5, Cu/ZSM-5 and Ni–Cu/ZSM-5 catalysts.

Material	XRF			EDS		
	Si/Al Ratio	Ni	Cu	Si/Al Ratio	Ni	Cu
ZSM-5	30.36	-	-	32.02	-	-
Ni/ZSM-5	28.75	9.83	-	29.04	10.10	-
Cu/ZSM-5	28.07	-	10.04	27.53	-	10.31
NiCu/ZSM-5	30.18	5.01	5.16	30.94	4.92	4.99

Cu/ZSM-5, maintain the characteristic coffin-like hexagonal morphology typical of the MFI zeolite framework [39], demonstrating that metal introduction does not disrupt the intrinsic crystal architecture of the parent material. The pristine ZSM-5 exhibits sharply defined crystal facets with a relatively smooth external surface, whereas incorporation of Ni and Cu leads to a progressive increase in surface roughness, indicative of metallic species anchored to the outer zeolite surface. This modification in surface texture is more pronounced in the Ni-Cu sample, where a more irregular topography suggests the simultaneous dispersion of both metals across the crystal surfaces. The preservation of the hexagonal crystal habit across all samples confirms that the impregnation and reduction procedures do not induce structural degradation, while the observed roughening of the external surface [37] provides additional evidence of successful metal deposition, consistent with the XRD results, which verified metal incorporation without compromising the zeolite framework.

The N_2 adsorption–desorption isotherms of ZSM-5, Cu/ZSM-5, Ni/ZSM-5, and NiCu/ZSM-5 (Figure 4a) exhibit type-IV behavior with H4-type hysteresis loops, indicating the simultaneous presence of micropores and slit-like mesopores that are typical of hierarchical zeolite frameworks. The preservation of the isotherm shape after incorporation of Cu, Ni, and the bimetallic Ni–Cu indicates that the impregnation does not alter the intrinsic MFI framework structure. This result is in line with prior studies reporting that secondary templating routes yield ZSM-5 with robust micro–mesopore networks that remain structurally stable upon metal loading.

Quantitative analysis of the textural properties (Table 2) provides deeper insight into how metal incorporation alters pore accessibility within the hierarchical structure. The parent ZSM-5 exhibits the highest BET surface area (407 $m^2.g^{-1}$) and micropore area (279 $m^2.g^{-1}$), reflecting its well-developed microporous network. Following Ni and Cu impregnation, S_{BET} decreases to 348 and 345 $m^2.g^{-1}$, respectively, due to partial occupation of micropores by dispersed metal species. The stronger reduction observed for Ni/ZSM-5 suggests more extensive penetration of Ni clusters into the micropore channels, consistent with their smaller ionic radius and greater dispersion. Interestingly, the bimetallic NiCu/ZSM-5 retains an intermediate S_{BET} (360 $m^2.g^{-1}$) but exhibits the highest total pore volume (0.282 $cm^3.g^{-1}$) and mesopore volume (0.183 $cm^3.g^{-1}$). These features indicate a synergistic interaction between Ni and Cu in which co-deposition limits excessive micropore blockage,

Table 2. Surface area and pore structure parameters of all catalysts.

Catalyst	Surface area ($m^2.g^{-1}$)			Volume @STP ($cm^3.g^{-1}$)			Pore Diameter (nm)	
	[a]BET	[b]Micro	[c]Ext	[d]Total	[e]Micro	[f]Meso		
ZSM-5	407.45	278.86	128.59	0.236	0.112	0.124	2.162	21.659
Ni/ZSM-5	348.22	238.89	109.33	0.253	0.101	0.152	2.341	21.659
Cu/ZSM-5	344.57	252.06	92.51	0.233	0.095	0.138	2.341	21.659
NiCu/ZSM-5	359.95	246.61	113.34	0.282	0.099	0.183	2.520	21.659

a = BET surface area; b = micropore area (T-plot); c = external surface area (a − b); d = total pore volume at P/Po = 0.99; e = micropore volume (T-plot); f = mesopore volume (total − micropore); g = pore size distribution (BJH desorption).

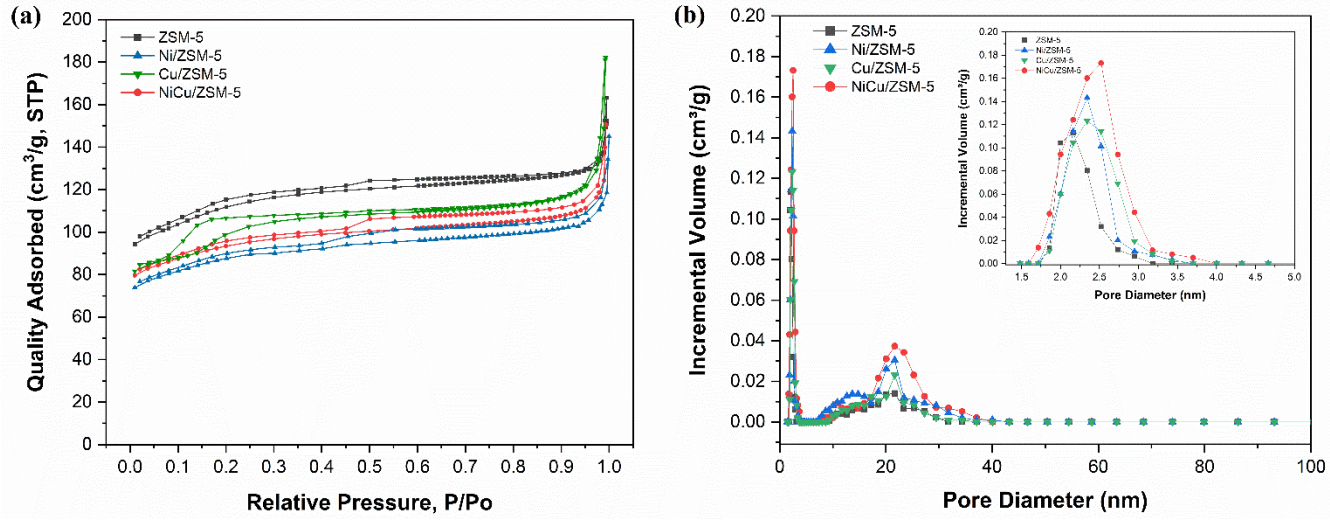

Figure 4. (a) N_2 adsorption-desorption isotherm and (b) Pore size distribution of ZSM-5 catalysts.

while simultaneously promoting the development of additional mesostructural voids. The partially preserved micropore area of NiCu/ZSM-5 (247 $m^2.g^{-1}$), compared with Ni/ZSM-5 (239 $m^2.g^{-1}$), further supports the notion that bimetallic impregnation maintains a larger fraction of the intrinsic micropore network relative to single-metal loading [40].

The BJH pore-size distribution profiles (Figure 4b) show dominant peaks at ~2.0 nm for all samples, confirming the retention of micropores associated with the MFI framework. A second distribution, centered at ~21–22 nm, originates from intercrystalline mesopores typically generated during the hierarchical synthesis of ZSM-5. After metal incorporation, the micropore volume decreases due to partial filling of pore mouths and channel intersections, particularly in Ni-containing catalysts. Conversely, the average pore diameter increases slightly in NiCu/ZSM-5 (2.52 nm), accompanied by the largest mesopore contribution, indicating that the formation of bimetallic domains promotes interparticle mesopore development without substantial collapse of the micropore network.

Overall, these textural characteristics demonstrate that all catalysts retain a hierarchical micro–mesoporous structure, while metal impregnation induces controlled modifications in pore-size distribution and accessibility. SEM and elemental analyses corroborate these findings, showing that metal species are dispersed across the external surface, forming small clusters that locally modify the pore environment. Consequently, although the surface area decreases after impregnation, the mesopore volume increases due to the formation of metal and bimetal aggregates that generate additional voids within the mesostructure. The enhancement of mesoporosity in the Ni- and NiCu-based catalysts is expected to improve the diffusion of larger molecules, such as lignin-derived substrates, thereby contributing to superior catalytic performance in subsequent reaction studies.

The summary of NH_3-Temperature Programmed Desorption NH_3-TPD profiles in Table 3 and Figure 5 clearly demonstrates that metal incorporation fundamentally alters the acidity characteristics of ZSM-5. Pristine ZSM-5 exhibits two characteristic desorption features [41]: a weak-acid peak at 217 °C and a strong-acid peak at 540 °C, consistent with Brønsted sites originating from framework Al. The absence of a discernible medium-acid region indicates that the unmodified zeolite possesses a relatively simple acidity pattern dominated by protonic Brønsted sites [42]. Upon metal impregnation, however, the desorption behavior changes markedly, both in the number of desorption bands and in the overall acidity distribution.

The incorporation of metal species markedly alters the acidity distribution of ZSM-5. In Ni/ZSM-5, a new medium-strength peak emerges at 311 °C, accompanied by a pronounced intensification of strong-acid signals at 541 and 663 °C. These changes indicate that Ni facilitates proton–metal exchange, generating additional Lewis sites while simultaneously reinforcing the remaining Brønsted sites. This trend aligns with the increase in total acidity to 0.756 $mmol.g^{-1}$ and the substantial decline in weak-acid fractions (from 45.64% to 15.25%), reflecting the

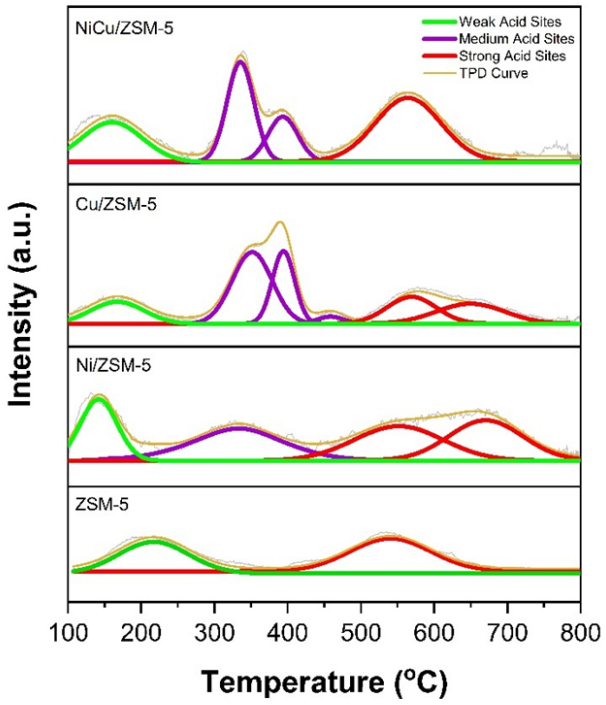

Figure 5. NH_3-TPD desorption curves of the ZSM-5 catalysts, represented by different coloured profiles.

Table 3. Summary of NH_3-TPD profiles and surface acid property for ZSM-5 catalysts.

Catalyst	Total acidity (mmol/g)	Acidic sites (mmol/g)			Acid cite content (%)			Peak position (°C)		
		Weak	Medium	Strong	Weak	Medium	Strong	Weak	Medium	Strong
ZSM-5	0.507	0.231	-	0.275	45.64	-	54.36	217	-	540
Ni/ZSM-5	0.756	0.115	0.240	0.401	15.25	31.74	53.01	148	311	541, 663
Cu/ZSM-5	0.686	0.098	0.380	0.208	14.24	55.43	30.33	168	353, 394	569, 650
NiCu/ZSM-5	0.912	0.104	0.265	0.543	11.40	29.05	59.53	160	336, 393	565

suppression of silanol-type sites and the growth of catalytically relevant medium- and strong-acid populations [43]. In contrast, Cu/ZSM-5 exhibits a distinct evolution in acidity. Although its total acidity also rises (0.686 mmol.g^{-1}), the most significant change occurs in the medium-acid region, which expands to 55.43% and manifests as two peaks at 353 and 394 °C. These features originate from the formation of abundant Lewis sites associated with well-dispersed Cu species [44]. The comparatively lower contribution of strong sites relative to Ni/ZSM-5 indicates that Cu predominantly interacts with external silanol groups [43] or surface defects, yielding a mixed acidity profile in which Brønsted sites are largely preserved while new Cu-derived Lewis sites are introduced.

The bimetallic NiCu/ZSM-5 system exhibits the most complex and synergistic acidity characteristics. The total acidity reaches the highest value among all catalysts (0.912 mmol.g^{-1}), indicating that co-impregnation of Ni and Cu produces a substantially larger and more diverse population of acid sites compared with monometallic counterparts. The medium-acid domain exhibits two distinct peaks at 336 and 393 °C, confirming the coexistence of Lewis sites from both metals with distinct coordination environments [44]. Strong-acid sites dominate the profile (59.53 %), with a major desorption peak at 565 °C, demonstrating that the framework Brønsted acidity is not only preserved but also reinforced through cooperative metal–zeolite interactions [42]. The reduced proportion of weak-acid sites (11.40 %) indicates that both metals suppress silanol-related acidity while promoting the formation of catalytically more robust acid sites.

Overall, the NH_3-TPD results corroborate the structural and surface characterizations and reveal that metal impregnation enhances total acidity while redistributing the strength of acid sites in a metal-dependent manner. Ni primarily increases the number of strong-acid sites while generating additional medium-strength sites via proton-exchange processes. In contrast, Cu predominantly enhances medium-acid sites by forming extensive Lewis sites from dispersed Cu species. The bimetallic system integrates both effects synergistically, producing the highest total acidity, the most balanced distribution of acid strengths, and the most intense high-temperature desorption behavior. Such an acidity pattern is highly advantageous for lignin and BPE conversion, as effective cleavage of C–O bonds and stabilization of reactive intermediates require a cooperative interplay between medium-strength Lewis sites and strong Brønsted acid sites.

3.2. Catalytic Test

Catalytic evaluations revealed that the bimetallic Ni–Cu/ZSM-5 catalyst displayed substantially higher activity than the parent ZSM-5, together with a marked performance improvement relative to the monometallic Ni/ZSM-5 and Cu/ZSM-5 catalysts. This superiority is consistent with its larger specific surface area, balanced elemental composition, and higher numbers and strengths of acid sites, as determined by NH_3-TPD analysis. In addition, XRD, FTIR, and SEM characterizations confirmed that the zeolite framework remained intact after impregnation, indicating that the enhanced activity arises from the introduced NiCu species rather than from changes in the zeolite morphology.

The physicochemical properties of catalysts and their correlation with activity were supported by the conversion percentages presented in Figure 6, which compared catalytic tests of two substrates. Figure 6a shows that the model

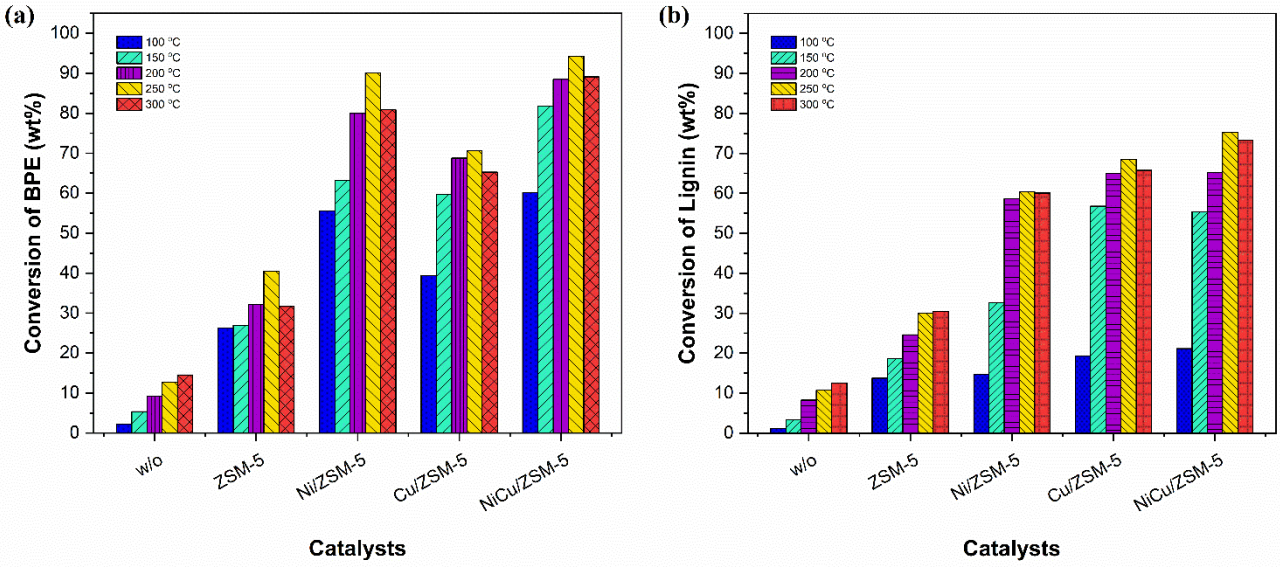

Figure 6. Catalytic activity in terms of substrate conversion for (a) BPE and (b) ILWB over various catalysts.

substrate, Benzyl Phenyl Ether (BPE), yielded 2.13–14.52% conversion in non-catalytic reactions and increased dramatically to 26.26–94.29% with catalysts, with the highest conversion (94.29%) achieved with NiCu/ZSM-5 at 250 °C. Furthermore, Figure 6b demonstrates that the real lignin substrate, isolated lignin from raw woody biomass waste (ILWB), produced significant conversions of 13.76–75.31% under catalytic conditions, with an optimum of 75% at 250 °C using the bimetallic NiCu/ZSM-5 catalyst. The mild optimal reaction temperature corresponds to the principles of green chemistry and aligns with the United Nations Sustainable Development Goals (SDGs) No. 9 and 12 [45].

As an organic molecule, the BPE reaction is strongly influenced by temperature; as expected, its conversion percentage is relatively high over the 150–300 °C reaction range, approaching 100%. Cleavage of C–O–C and aryl ether linkages has been reported to take place within this temperature window [46]. In contrast, native lignin exhibits reactivity between 200 °C and 400 °C over longer reaction times. At this stage, primary pyrolysis and ether bond cleavage, particularly of the *α*–O–4 and *β*–O–4 linkages, dominate the reaction pathways. When the temperature exceeds 400 °C, radical-based processes become more dominant, leading to extensive structural rearrangements within the lignin. Within this temperature interval, C–C bond scission takes place, leading to the generation of oligomeric and monomeric species [47]. Accordingly, the formation of monomers and phenolic products from native lignin (kraft lignin) using a CoMo/SBA-15 catalyst under supercritical ethanol conditions was demonstrated by Rana *et al.* in the temperature interval of 240–320 °C [48].

Although an optimal reaction temperature is required to activate cleavage of the C–O–C bond in BPE and the ether linkages in native lignin, temperature alone is insufficient to control product yield. Under non-catalytic conditions, lignin depolymerization may proceed via multiple competitive reaction pathways, leading to side reactions or thermal degradation at elevated temperatures that generate coke and tar, thereby reducing the yield of phenols and other oxygenated aromatic compounds [49]. Therefore, the presence of a suitable catalyst is crucial to direct the reaction toward the formation of desired phenolic products, particularly phenol and vanillin. The acidity distribution and textural properties of the catalyst—especially accessibility and pore structure —are key factors determining product yield because they influence substrate accessibility and the diffusion of intermediates and phenolic products [50]. Although higher temperatures enhance catalytic activity and proton transfer from zeolitic acid sites, excessively high temperatures may trigger secondary reactions and decrease the product yield.

In principle, the catalytic reaction of BPE proceeds through a hydrogenolysis stage that produces phenol, followed by a hydrodeoxygenation (HDO) step that converts phenol into vanillin. Figure 7 presents the yield percentages of the target compounds, namely phenol and vanillin. Among the two substrates compared, phenol production was higher with BPE than with ILWB, although the vanillin yield remained relatively comparable. This finding is consistent with the fact that simple model ether compounds are more easily depolymerized than highly polycondensed native lignin [51]. Meanwhile, vanillin exhibited a nearly equivalent yield to phenol in the conversion of ILWB, indicating that the more complex lignin structure tends to yield a broader distribution of phenolic products [52]. The catalytic performance in both BPE and ILWB conversions is primarily governed by catalyst design rather than by temperature control alone, as the physicochemical properties and active-site distribution direct the reaction pathways toward high-value phenolic products such as phenol and vanillin.

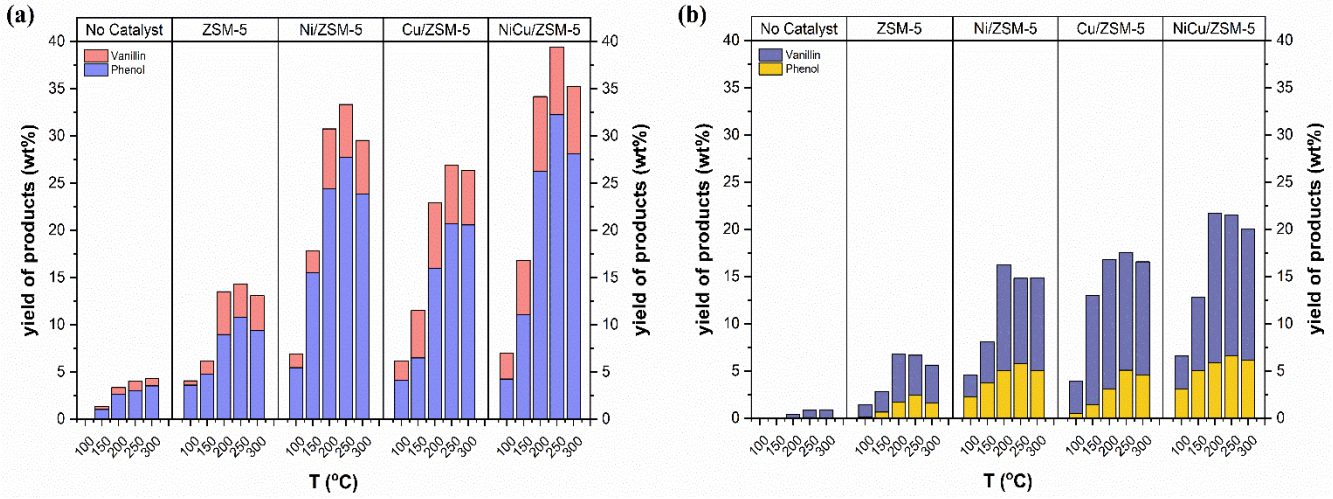

Figure 7. Catalytic activity in terms of product yields for (a) BPE and (b) ILWB substrates.

The catalytic activity presented in Figure 7 covers all types of catalysts tested. Under non-catalytic conditions, no detectable product yield was obtained. With the parent ZSM-5, the formation of phenol and vanillin products proceeded more favorably than under non-catalytic conditions. For the BPE substrate, phenol and vanillin yields reached 10.76% at 250 °C and 4.53% at 200 °C, respectively, while for the ILWB substrate, phenol and vanillin yields were 2.41% at an optimum temperature of 250 °C and 5.10% at 200 °C, respectively. The consistent temperature trend observed across all catalysts is likely due to the higher activity of phenolic intermediates transforming into vanillin at 200 °C [53]. Beyond this temperature, further degradation of vanillin into carboxylic acids or other oxidation products might occur; however, at 250 °C, C–O–C bond cleavage in BPE is maximized, enhancing phenol formation [18,28].

This study aligns with previous reports indicating that ZSM-5 facilitates the formation of phenol and oxygenated aromatics from both lignin-derived model compounds and native lignin [28,50]. Hierarchical ZSM-5 catalysts provide Brønsted–Lewis acid sites that facilitate multiple reactions, adsorb, and activate substrates [54]. As evidenced by the physicochemical properties shown in the NH_3-TPD profiles, ZSM-5 exhibits two desorption peaks representing strong acid sites associated with framework aluminum (tending toward Lewis acidity) and weak acid sites associated with Si–OH groups (tending toward Brønsted acidity).

The modification of ZSM-5 with monometallic Ni and Cu introduced additional catalytic acidity, as indicated by the appearance of a new peak in the high-temperature region [41] and changes in the dominant composition of acid sites, thereby significantly enhancing catalytic performance compared to the parent ZSM-5. This phenomenon is compatible with the present findings, where the use of Ni/ZSM-5 catalyst yielded 27.75% phenol and 6.36% vanillin from the BPE substrate, and 5.77% phenol and 11.25% vanillin from native lignin. Similarly, the Cu/ZSM-5 catalyst produced slightly different, but comparable results, with phenol and vanillin yields of 20.70% and 6.95%, respectively, while the ILWB substrate generated 5.09% phenol and 13.70% vanillin. Specifically, these results suggest that incorporating monometallic Ni results in a higher molar acidity than Cu modification. This result arises from the more substantial contribution of Lewis acid sites associated with Ni species, which provide greater reinforcement of catalytic activity and improve reaction performance [55].

With the incorporation of bimetallic Ni–Cu, the conversion reactions of BPE and ILWB proceeded readily under the optimal catalytic conditions at 250 °C. The considerably higher conversion tendency confirms that the activity of Ni–Cu is not derived from a simple combination of monometallic Ni and Cu species but rather reflects a synergistic effect at the metal surface. Previous studies indicate that Ni predominantly promotes C–O bond cleavage and hydrogen transfer, whereas Cu suppresses excessive hydrogenolysis and mitigates over-reduction of aromatic intermediates [22,56]. The formation of a Ni–Cu alloy balances these two functions by electronically tuning the reactive transition-metal d orbitals at the active sites, thereby enhancing the adsorption–desorption behavior of reactants and products and thereby facilitating hydrogen activation and electron transfer (redox) for both hydrogenolysis and HDO processes [28].

Interestingly, the superior performance of the bimetallic Ni–Cu/ZSM-5 catalyst is attributed to the synergistic effects of the interaction between Ni–Cu metal sites and the hierarchical acidic framework of ZSM-5. Ni–Cu/ZSM-5 is known to possess Lewis acid sites arising from Na^+, Al^{3+}, Ni^{2+}, and Cu^{2+} ions, while hydroxyl groups on the zeolite framework generate Brønsted acid sites [42]. This phenomenon is consistent with the NH_3-TPD analysis, which shows that Ni–Cu/ZSM-5 exhibits the highest molar acidity and an optimal distribution of Brønsted–Lewis acid sites. Consequently, the optimized conversion of BPE and lignin affords maximum yields of 32.25% phenol and 7.95% vanillin for the BPE substrate, and 6.61% phenol and 15.85% vanillin for the ILWB substrate. Overall, the synergistic effect of the Ni–Cu/ZSM-5 catalyst enhances the yields and selectivities of phenol and vanillin.

In addition to phenol and vanillin, the reaction products obtained from both BPE and ILWB substrates are expected to consist of a complex mixture of oxygenated aromatic compounds, oligomeric lignin fragments, and unidentified species, particularly in the case of native lignin conversion [57,58]. Previous studies have reported the formation of other low-molecular-weight products, such as benzene, cyclohexane, cyclohexanol, and cyclohexanone, during lignin hydrogenolysis and hydrodeoxygenation over metal-supported catalysts [28,52]. The formation of these compounds is generally associated with extensive hydrogenation and deep deoxygenation pathways, which may partially account for the relatively low yields of the target phenolic products observed under certain reaction conditions.

Furthermore, variations in conversion percentages and product yields were strongly determined by the elemental constitution and pore architecture of the catalysts, as revealed by EDS–XRF and BET analyses. Elemental data confirm that the ratio of active metals uniformly distributed on the ZSM-5 surface directly affects the extent of cleavage of C–O and C–C linkages

[59]. Catalysts containing mono- and bimetallic species exhibit a higher number of redox-active sites, thereby promoting hydrogenolysis and HDO pathways and accelerating the depolymerization of both model compound and lignin. The Si/Al ratio likewise governs the acidity and catalytic activity [60], which explains the superior performance of the bimetallic Ni–Cu/ZSM-5 catalyst in this study compared to the parent ZSM-5 and its monometallic counterparts Ni/ZSM-5 and Cu/ZSM-5. On the other hand, the pore architecture, as defined by BET surface area, cumulative pore volume, and the distribution of mesopores from BET analysis, leads to significant distinctions in the catalyst's ability to accommodate bulky reactant molecules, such as benzyl phenyl ether (BPE) and isolated lignin from raw woody biomass waste (ILWB).

An increase in the mesopore ratio in several samples, such as Ni–Cu/ZSM-5 and Ni/ZSM-5, enhances internal diffusion, minimizes mass transfer limitations, and allows aromatic molecules with sizes approaching the diffusion limit of ZSM-5 to interact more readily with active sites [49,61]. This behavior arises because the interconnected 10-ring channel structure of ZSM-5 can direct the orientation of reactants and products diffusing through the pore channels. At the same time, the additional mesoporosity in hierarchical ZSM-5 further reduces diffusion constraints, thereby improving the utilization of intra-pore acid sites and the overall catalytic reaction efficiency. Interestingly, catalysts with higher total surface area in ZSM-5 but without dominant mesopore surface area and volume tend to exhibit lower conversion due to restricted catalytic access and reduced mass transfer efficiency during reaction. In contrast, Ni–Cu/ZSM-5, which possesses a dominant mesoporous surface area and volume, provides more open diffusion pathways for BPE and dissolved lignin, thus enabling maximal yields of phenol and vanillin. Beyond activity enhancement, the practical applicability of such heterogeneous catalysts is also closely related to their structural stability.

Despite the heterogeneous nature of the Ni–Cu/ZSM-5 catalyst, catalyst reuse and regeneration experiments were not conducted in the present study. This work was primarily designed to elucidate structure–property–performance relationships through catalyst synthesis, comprehensive physicochemical characterization, and evaluation of catalytic performance in a single reaction cycle. The absence of a recyclability assessment is therefore acknowledged as a limitation of the present study. Nevertheless, the preserved zeolite framework and the stable incorporation of Ni–Cu species, as evidenced by XRD and FTIR analyses, suggest that the catalyst possesses sufficient structural robustness for potential reuse. A systematic investigation of catalyst stability, recyclability, and regeneration behavior will be the focus of future work to further evaluate its applicability in practical lignin valorization processes.

Overall, the combination of elemental composition and textural parameters accounts for the differences in catalytic behavior under identical reaction conditions. An optimal metal composition together with a well-organized pore structure enhances the synergistic effect on catalytic performance. The metal phase provides hydrogen activation and redox-active centers for electron transfer in hydrogenolysis and hydrodeoxygenation (HDO) processes [28], whereas the acid sites and pore framework of ZSM-5 ensure optimal adsorption, orientation, and diffusion of reactants [42,62,63]. The integration of these factors enhances the catalyst's synergistic nature, thereby promoting the upgrading of lignin and its model compound into high-value phenolic products. These findings highlight that the design of metal composition and pore structure must be considered simultaneously with acid strength, as all three act synergistically to control reaction pathways, conversion levels, and product yields.

The findings of this study demonstrate that the conversion of BPE and lignin is highly dependent on the synergistic interaction effects between zeolitic acid sites and metallic redox sites. This trend is consistent with several previous reports demonstrating that combining acid and redox functions can lower the activation energy for hydrogenolysis and enhance product formation. For example, bimetallic Pd/Co catalysts achieved 88% BPE conversion with a 37% phenol yield at 240 °C for 180 min [18], while Yan et al. reported the conversion of organosolv lignin over Ni–Fe–Mo_2C/AC to give 19% H-type phenols at 260 °C for 4 h [19]. In another study, Ni/Al-SBA-15 converted lignin from olive tree prunings at 140 °C for 30 min, affording 0.20% vanillin and 0.15% 3,4-dimethoxyphenol [64]. Hydrogenolysis of BPE over $NiCu/Al_2O_3$ produced phenol yields of 5.12–37.42% at 200 °C for 2 h [21], whereas HDO of BPE using NiMo/γ-alumina–USY-zeolite at 320 °C for 6 h led to >99% BPE conversion with 13% phenol yield and 44.5% total yield of deoxygenated aromatics [23].

The findings from these earlier studies demonstrate that catalysts based on metallic redox sites combined with acid sites on porous materials generally produce phenol or vanillin at higher temperatures and longer reaction times than those applied in the present work, particularly when raw lignin with high structural heterogeneity is involved. In contrast, in this study, the synergistic effect of the Ni–Cu/ZSM-5 catalyst provides superior performance for both BPE and ILWB lignin, with an increased

proportion of phenolic products under lower temperatures and shorter reaction times, i.e., relatively mild conditions. This observation suggests that integrating Brønsted–Lewis acid sites with bimetallic redox sites can effectively direct the reaction toward higher yields of phenol and vanillin.

A previous investigation by Ramadhani et al. successfully converted DPE using Co- and Mo-based monometallic ZSM-5 catalysts at 200 °C and 250 °C [28]. The process afforded phenol and vanillin yields of 31% and 7%, respectively, but it did not involve direct comparison with isolated native lignin from biomass, nor did it investigate a bimetallic system. In addition, the Co- and Mo-modified ZSM-5 catalysts were designed for the conversion of the model compound diphenyl ether (DPE). In contrast, the present study compares a model compound with real lignin using BPE and ILWB, and examines the Ni–Cu bimetallic system in parallel with its monometallic counterparts. Accordingly, this work demonstrates that phenol and vanillin yields in the catalytic conversion of the BPE–ILWB system, representing lignin model and native lignin, correlate strongly with the synergistic catalytic effect, which is crucial for enhancing performance. Therefore, this study recommends Ni–Cu/ZSM-5, synthesized with a higher acid site density, an appropriate metal loading, and substantial mesoporosity, as a promising catalyst for lignin conversion under relatively mild conditions (200–250 °C for 30 min).

Overall, the selectivity trends observed in Figures 6 and 7 are governed by the interplay between catalyst acidity, metal functionality, and substrate complexity. The balanced Brønsted–Lewis acidity and enhanced metal–support interactions in Ni-, Cu-, and especially Ni–Cu-modified ZSM-5 promote C–O–C bond cleavage and controlled hydrogenation [59], favoring the formation of phenol and vanillin from BPE. In contrast, the structurally complex ILWB undergoes competing depolymerization and secondary reactions [8], resulting in broader product distributions and lower apparent selectivity. These results indicate that catalyst physicochemical properties and the intrinsic reactivity of the lignin-derived substrate jointly dictate product selectivity.

3.3. Proposed Reaction Mechanism

Based on the observed catalytic performance, physicochemical properties of the synthesized catalysts, and comparison with previously reported systems, a plausible reaction mechanism for the transformation of the lignin model compound benzyl phenyl ether (BPE) and isolated lignin from raw woody biomass waste (ILWB) over the bimetallic Ni–Cu/ZSM-5 catalyst can be proposed. The reaction pathway illustrated in Figure 8 is inferred from acidity–porosity analyses (NH_3-TPD and BET), elemental composition (EDS–XRF), product distribution trends, and established mechanistic insights reported in the literature, rather than from direct spectroscopic observation of reaction intermediates.

The reaction is presumed to proceed via a bifunctional catalytic pathway, involving the cooperative roles of acid sites, hierarchical pore architecture of ZSM-5, and redox-active metal centers associated with the Ni–Cu phase. Initially, BPE molecules are adsorbed onto the catalyst surface through interactions between the ether oxygen and Brønsted and Lewis acid sites of the ZSM-5 framework. Proton donation from Brønsted acid sites and polarization by Lewis acid centers are widely reported to weaken the C–O–C linkage, thereby facilitating ether bond activation [42,62,63].

Following substrate activation, the Ni–Cu phase is proposed to function as a hydrogenation–deoxygenation center. In the absence of external hydrogen gas, reactive hydrogen species are plausibly generated in situ through interactions involving surface acid functionalities and the ethanol solvent, which acts as a hydrogen donor. Partial reduction at the metal surface may lead to the formation of adsorbed hydrogen species, commonly described in the literature as Ni–H and Cu–H species, which are capable of participating in hydrogenolysis reactions [55]. Such species are often proposed to migrate across the catalyst surface via hydrogen spillover, facilitating selective cleavage of the activated α-O-4 ether bonds. This step yields phenoxy and benzyl-derived intermediates, which subsequently stabilize to form phenol as the dominant product. The presence of bimetallic Ni–Cu sites is reported to modify the electronic environment of the metal centers, optimizing adsorption strength and lowering the apparent activation barrier for C–O bond scission relative to monometallic systems [65].

Further transformation of selected intermediates to vanillin is proposed to occur through controlled hydrodeoxygenation and oxidation pathways, consistent with the observed product distribution. Lewis acid sites may contribute to the activation of hydroxyl-containing intermediates, while the Ni–Cu bimetallic phase mediates redox processes involving surface hydrogen species. Ethanol is suggested to play a dual role as solvent and hydrogen donor, facilitating side-chain oxidation steps that lead to aldehyde formation characteristic of vanillin [28,50]. The hierarchical pore structure of ZSM-5 further enhances diffusion of bulky lignin fragments and reaction intermediates, thereby reducing mass-transfer limitations and suppressing secondary condensation or repolymerization reactions.

Overall, the proposed mechanism highlights the synergistic interplay between zeolitic acid sites, redox-active Ni–Cu centers, and hierarchical porosity. Nickel contributes predominantly to hydrogen activation, while copper moderates hydrogenolysis severity and enhances electronic interactions, resulting in balanced selectivity toward phenol and vanillin. It should be emphasized that this mechanism is presented as a plausible reaction pathway supported by observed catalytic trends and literature precedent, rather than as direct post-reaction spectroscopic evidence of surface intermediates.

4. Conclusions

The findings of this work reveal that the bimetallic Ni–Cu/ZSM-5 catalyst displays markedly enhanced activity for the hydrogenolysis and hydrodeoxygenation of BPE and ILWB. The synergistic effect separating the bimetallic active sites and the porous ZSM-5 matrix results in significantly higher conversions and product yields of phenol and vanillin than the monometallic Ni/ZSM-5 and Cu/ZSM-5 catalysts, as well as the parent ZSM-5. This behavior arises from the combined physicochemical properties, namely enhanced acidity, improved metal

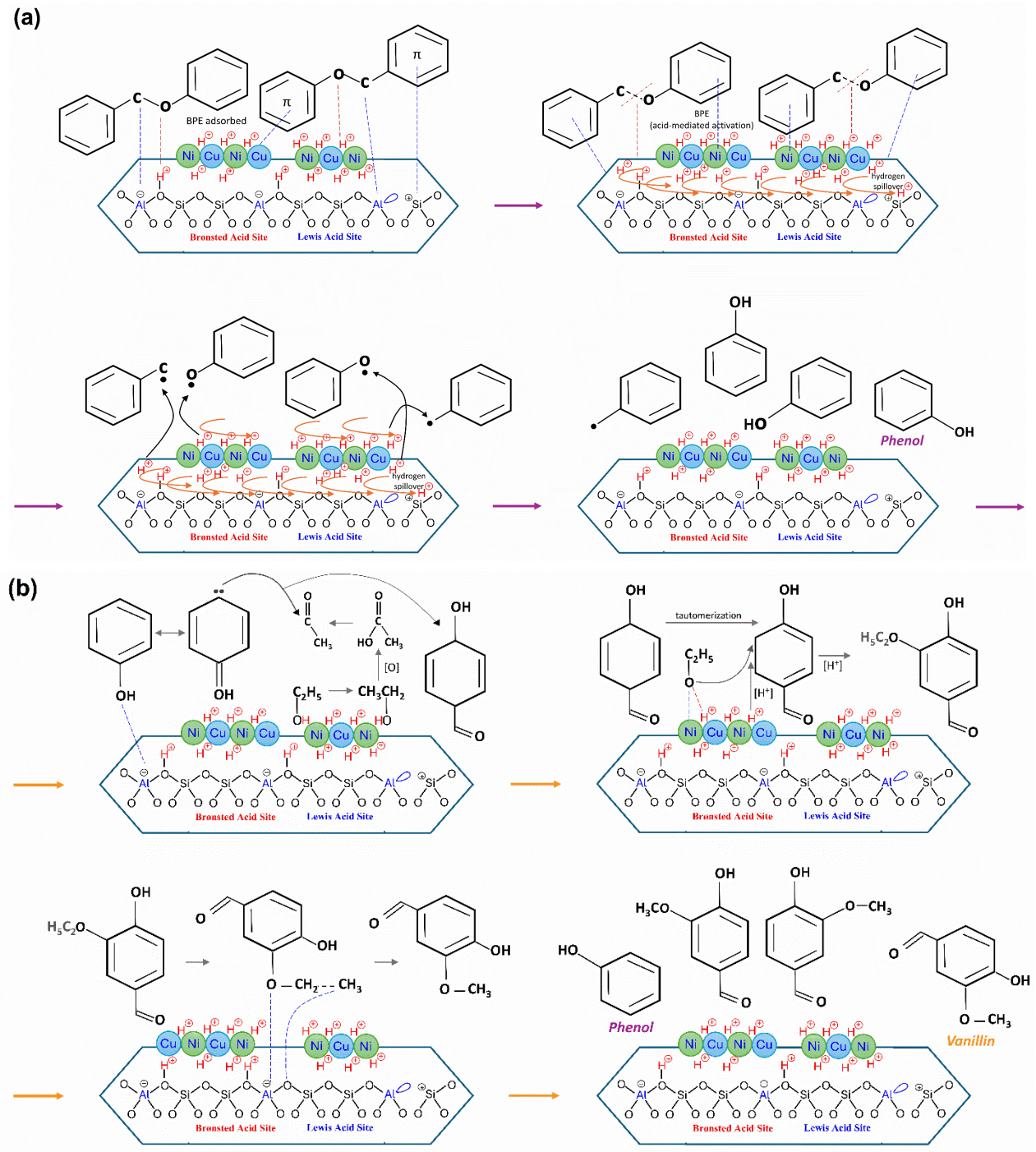

Figure 8. Proposed mechanism for the formation of (a) phenol and (b) vanillin from BPE over the bimetallic Ni–Cu/HZSM-5 catalyst.

dispersion, and hierarchical porosity, which collectively promote substrate activation and diffusion. The hierarchical bimetallic Ni–Cu/ZSM-5 catalyst is verified as the most effective system in this reaction, achieving up to 94.29% conversion for the BPE substrate at 250 °C with the highest phenol yield (32.25%), and 75.31% conversion for the native ILWB lignin substrate with the highest vanillin yield (15.85%) after 30 min of reaction. In addition, the results indicate that reaction temperature significantly influences both conversion and the yields of the resulting phenolic products. Overall, this work offers valuable guidance for designing bifunctional catalytic systems for lignin valorization and for using BPE as a lignin model under relatively mild reaction conditions, while also highlighting the potential for the sustainable production of high-value phenolic chemicals from renewable biomass feedstocks. Future studies will focus on catalyst stability and recyclability to assess the long-term performance of the Ni–Cu/ZSM-5 system.

Acknowledgment

This work was supported by the Ministry of Research, Technology, and Higher Education of the Republic of Indonesia through the Pendidikan Magister menuju Doktor untuk Sarjana Unggul (PMDSU) research grant No. NKB-436/UN2.RST/HKP.05.00/2020.

CRedit Author Statement

Author Contributions: Arnia Putri Pratama: Formal analysis, Validation, Formal analysis, Investigation Data curation, Writing – Original Draft, Visualization, Project administration. Iman Abdullah: Methodology, Supervision. Yuni Krisyuningsih Krisnandi: Conceptualization, Methodology, Writing – Review & Editing, Supervision, Funding acquisition. All authors have read and agreed to the published version of the manuscript.

References

[1] Haq, I., Mazumder, P., Kalamdhad, A.S. (2020). Recent advances in removal of lignin from paper industry wastewater and its industrial applications – A review. *Bioresource Technology*, 312 (April), 123636. DOI: 10.1016/j.biortech.2020.123636.

[2] Rasid, N.S.A., Shamjuddin, A., Amin, N.A.S. (2021). Chemical and structural changes of ozonated empty fruit bunch (EFB) in a ribbon-mixer reactor. *Bulletin of Chemical Reaction Engineering & Catalysis*, 16(2), 383–395. DOI: 10.9767/bcrec.16.2.10506.383-395.

[3] Chio, C., Sain, M., Qin, W. (2019). Lignin utilization: A review of lignin depolymerization from various aspects. *Renewable and Sustainable Energy Reviews*, 107(December 2018), 232–249. DOI: 10.1016/j.rser.2019.03.008.

[4] Bajwa, D.S., Pourhashem, G., Ullah, A.H., Bajwa, S.G. (2019). A concise review of current lignin production, applications, products and their environment impact. *Industrial Crops and Products*, 139 (June), 111526. DOI: 10.1016/j.indcrop.2019.111526.

[5] Ragauskas, A.J., Beckham, G.T., Biddy, M.J., Chandra, R., Chen, F., Davis, M.F., Davison, B.H., Dixon, R.A., Gilna, P., Keller, M., Langan, P., Naskar, A.K., Saddler, J.N., Tschaplinski, T.J., Tuskan, G.A., Wyman, C.E. (2014). Lignin valorization: Improving lignin processing in the biorefinery. *Science*, 344 (6185) DOI: 10.1126/science.1246843.

[6] Weng, C., Peng, X., Han, Y. (2021). Depolymerization and conversion of lignin to value-added bioproducts by microbial and enzymatic catalysis. *Biotechnology for Biofuels*, 14(1), 1–22. DOI: 10.1186/s13068-021-01934-w.

[7] Attard, T., Hunt, A., Matharu, A., Houghton, J., Polikarpov, I. (2014). Introduction to Chemicals from Biomass, Second Edition. In: *Introduction to Chemicals from Biomass: Second Edition*. pp. 31–52. DOI: 10.1002/9781118714478.ch2.

[8] Chen, X., Weixiang, G., Tsang, C.-W., Haoquan, H., Changhai, L. (2019). Lignin Valorizations with Ni Catalysts for Renewable Chemicals and Fuels Productions. *Catalysts*, 9(6), 488–527.

[9] Díez, D., Urueña, A., Piñero, R., Barrio, A., Tamminen, T. (2020). Determination of hemicellulose, cellulose, and lignin content in different types of biomasses by thermogravimetric analysis and pseudocomponent kinetic model (TGA-PKM Method). *Processes*, 8(9). DOI: 10.3390/pr8091048.

[10] Xu, Y., Guo, L., Zhang, H., Zhai, H., Ren, H. (2019). Research status, industrial application demand and prospects of phenolic resin. *RSC Advances*, 9(50), 28924–28935. DOI: 10.1039/c9ra06487g.

[11] Qiang, H., Wang, J., Liu, H., Zhu, Y. (2023). From vanillin to biobased aromatic polymers. *Polymer Chemistry*, 14(37), 4255–4274. DOI: 10.1039/d3py00767g.

[12] Ben, H., Ragauskas, A.J. (2011). Pyrolysis of kraft lignin with additives. *Energy and Fuels*, 25(10), 4662–4668. DOI: 10.1021/ef2007613.

[13] Kantarelis, E., Javed, R., Stefanidis, S., Psarras, A., Iliopoulou, E., Lappas, A. (2019). Engineering the Catalytic Properties of HZSM-5 by Cobalt Modification and Post-synthetic Hierarchical Porosity Development. *Topics in Catalysis*, 62(7–11), 773–785. DOI: 10.1007/s11244-019-01179-w.

[14] Naron, D.R., Collard, F.X., Tyhoda, L., Görgens, J.F. (2019). Production of phenols from pyrolysis of sugarcane bagasse lignin: Catalyst screening using thermogravimetric analysis – Thermal desorption – Gas chromatography – Mass spectroscopy. *Journal of Analytical and Applied Pyrolysis*, 138(December 2018), 120–131. DOI: 10.1016/j.jaap.2018.12.015.

[15] Zhang, C.T., Zhang, L., Li, Q., Wang, Y., Liu, Q., Wei, T., Dong, D., Salavati, S., Gholizadeh, M., Hu, X. (2019). Catalytic pyrolysis of poplar wood over transition metal oxides: Correlation of catalytic behaviors with physiochemical properties of the oxides. *Biomass and Bioenergy*, 124 (February), 125–141. DOI: 10.1016/j.biombioe.2019.03.017.

[16] Sun, L., Wang, Z., Chen, L., Yang, S., Xie, X., Gao, M., Zhao, B., Si, H., Li, J., Hua, D. (2020). Catalytic fast pyrolysis of biomass into aromatic hydrocarbons over Mo-modified ZSM-5 catalysts. *Catalysts*, 10(9), 1–10. DOI: 10.3390/catal10091051.

[17] Shen, Y., Liu, C., Cui, C., Ren, H., Gu, M., Liu, H., Zhou, Z., Qi, F. (2024). Effect of Cu-modified HZSM-5 zeolites on catalytic pyrolysis of lignin to producing aromatic hydrocarbons. *Fuel*, 361 (October), 130719. DOI: 10.1016/j.fuel.2023.130719.

[18] Mauriello, F., Ariga-Miwa, H., Paone, E., Pietropaolo, R., Takakusagi, S., Asakura, K. (2020). Transfer hydrogenolysis of aromatic ethers promoted by the bimetallic Pd/Co catalyst. *Catalysis Today*, 357, 511–517. DOI: 10.1016/j.cattod.2019.06.071.

[19] Yan, B., Lin, X., Chen, Z., Cai, Q., Zhang, S. (2021). Selective production of phenolic monomers via high efficient lignin depolymerization with a carbon based nickel-iron-molybdenum carbide catalyst under mild conditions. *Bioresource Technology*, 321, 124503. DOI: 10.1016/j.biortech.2020.124503.

[20] Jeong, S., Yang, S., Kim, D.H. (2017). Depolymerization of Protobind lignin to produce monoaromatic compounds over Cu/ZSM-5 catalyst in supercritical ethanol. *Molecular Catalysis*, 442, 140–146. DOI: 10.1016/j.mcat.2017.09.010.

[21] Wu, F.P., Zhao, Y.P., Fu, Z.P., Qiu, L. Le, Xiao, J., Li, J., Liu, F.J., Cao, J.P. (2023). Catalytic transfer hydrogenolysis mechanism of benzyl phenyl ether over NiCu/Al2O3 using isopropanol as hydrogen source. *Fuel Processing Technology*, 250, 107874. DOI: 10.1016/j.fuproc.2023.107874.

[22] Korányi, T.I., Huang, X., Coumans, A.E., Hensen, E.J.M. (2017). Synergy in Lignin Upgrading by a Combination of Cu-Based Mixed Oxide and Ni-Phosphide Catalysts in Supercritical Ethanol. *ACS Sustainable Chemistry and Engineering*, 5(4), 3535–3543. DOI: 10.1021/acssuschemeng.7b00239.

[23] Salam, M.A., Arora, P., Ojagh, H., Cheah, Y.W., Olsson, L., Creaser, D. (2019). NiMoS on alumina-USY zeolites for hydrotreating lignin dimers: Effect of support acidity and cleavage of C-C bonds. *Sustainable Energy and Fuels*, 4(1), 149–163. DOI: 10.1039/c9se00507b.

[24] Bensafi, B., Chouat, N., Djafri, F. (2023). The universal zeolite ZSM-5: Structure and synthesis strategies. A review. *Coordination Chemistry Reviews*, 496 (July 2022) DOI: 10.1016/j.ccr.2023.215397.

[25] Herlina, I., Krisnandi, Y.K., Ridwan, M. (2024). Oxidation of 5-hydroxymethylfurfural into 2,5-furandicarboxylic acid over CuO and NiO modified natural sourced hierarchical ZSM-5. *South African Journal of Chemical Engineering*, 47 (December 2022), 75–82. DOI: 10.1016/j.sajce.2023.10.011.

[26] Helmi, M.R.A., Rahayu, D.U.C., Pratama, A.P., Khatrin, I., Ramadhani, A.N., Krisnandi, Y.K. (2023). Comparative study of microwave-assisted versus conventional heated reactions of biomass conversion into levulinic acid over hierarchical Mn3O4/ZSM-5 zeolite catalysts. *Carbon Resources Conversion*, 6(3), 245–252. DOI: 10.1016/j.crcon.2023.02.005.

[27] Sofyani, U., Krisnandi, Y.K., Abdullah, I. (2022). Synthesis and Characterization of Mesoporous Carbon Supported Ni-Ga Catalyst for Low-Pressure CO2 Hydrogenation. *Bulletin of Chemical Reaction Engineering & Catalysis*, 17(2), 278–285. DOI: 10.9767/bcrec.17.2.13377.278-285.

[28] Ramadhani, A.N., Abdullah, I., Krisnandi, Y.K. (2022). Effect of Physicochemical Properties of Co and Mo Modified Natural Sourced Hierarchical ZSM-5 Zeolite Catalysts on Vanillin and Phenol Production from Diphenyl Ether. *Bulletin of Chemical Reaction Engineering & Catalysis*, 17(1), 225–239. DOI: 10.9767/bcrec.17.1.13372.225-239.

[29] Pratama, A.P., Krisnandi, Y.K., Abdullah, I. (2020). Catalytic depolymerization of lignin from wood waste biomass over natural sourced ZSM-5 catalysts. *IOP Conference Series: Materials Science and Engineering*, 902(1) DOI: 10.1088/1757-899X/902/1/012051.

[30] Herlina, I., Krisnandi, Y.K., Ridwan, M. (2025). Production of 2,5-furandicarboxylic acid (FDCA) from delignified rice husk waste over Cu and Ni metal-organic framework catalyst. *Case Studies in Chemical and Environmental Engineering*, 11 (March), 101233. DOI: 10.1016/j.cscee.2025.101233.

[31] Gille, T., Seifert, M., Marschall, M.S., Bredow, S., Schneider, T., Busse, O., Reschetilowski, W., Weigand, J.J. (2021). Conversion of oxygenates on H-ZSM-5 zeolites—effects of feed structure and Si/Al ratio on the product quality. *Catalysts*, 11(4), 1–20. DOI: 10.3390/catal11040432.

[32] Shahzad, A., Ahmad, I., Manzoor, A., Kashif, M., Ahsan, M., He, M., Razzokov, J. (2023). Synthesis of nickel nanowires (Ni-NWs) as high ferromagnetic material by electrodeposition technique. *Heliyon*, 9(1), e12576. DOI: 10.1016/j.heliyon.2022.e12576.

[33] Xu, H., Li, Q., Bi, Z., Xu, D., Guo, Y. (2025). Sustainable lactic acid production from glycerol via hydrothermal catalysis over highly dispersed cu nanoparticles on bio-tar derived carbon. *Journal of Environmental Chemical Engineering*, 13 (September) DOI: 10.1016/j.jece.2025.119275.

[34] Smail, H., Rehan, M., Shareef, K., Ramli, Z., Nizami, A.-S., Gardy, J. (2019). Synthesis of Uniform Mesoporous Zeolite ZSM-5 Catalyst for Friedel-Crafts Acylation. *ChemEngineering*, 3(2), 35. DOI: 10.3390/chemengineering3020035.

[35] Srihasam, S., Thyagarajan, K., Korivi, M., Lebaka, V.R., Mallem, S.P.R. (2020). Phytogenic generation of NiO nanoparticles using stevia leaf extract and evaluation of their in-vitro antioxidant and antimicrobial properties. *Biomolecules*, 10(1) DOI: 10.3390/biom10010089.

[36] Rita, A., Sivakumar, A., Martin Britto Dhas, S.A. (2019). Influence of shock waves on structural and morphological properties of copper oxide NPs for aerospace applications. *Journal of Nanostructure in Chemistry*, 9(3), 225–230. DOI: 10.1007/s40097-019-00313-0.

[37] Mohamed, A., Shaban, M., Kordy, M.G.M., Al-senani, G.M., Eissa, M.F., Hamdy, H. (2024). Fabrication and characterization of NiCu/GO and NiCu/rGO nanocomposites for fuel cell application. *RSC Advances*, 14, 6776–6792. DOI: 10.1039/D3RA07822A.

[38] Marguí, E., Queralt, I., de Almeida, E. (2022). X-ray fluorescence spectrometry for environmental analysis: Basic principles, instrumentation, applications and recent trends. *Chemosphere*, 303 (P1), 135006. DOI: 10.1016/j.chemosphere.2022.135006.

[39] Ma, P., Zhou, H., Li, Y., Wang, M., Nastase, S.A.F., Zhu, M., Cui, J., Cavallo, L., Cheng, K., Dutta Chowdhury, A. (2024). Selectivity descriptors of the catalytic n-hexane cracking process over 10-membered ring zeolites. *Chemical Science*, 15(30), 11937–11945. DOI: 10.1039/d4sc00603h.

[40] Shen, Z., Li, W., Jin, J., Lu, Z., Wang, L., Jiang, Y., Yuan, L. (2025). Highly efficient oxidation of methane into methanol over Ni-promoted Cu/ZSM-5. *RSC Advances*, 15(11), 8244–8252. DOI: 10.1039/d5ra01115a.

[41] Denardin, F.G., Perez-Lopez, O.W. (2020). Methane dehydroaromatization over Fe-M/ZSM-5 catalysts (M= Zr, Nb, Mo). *Microporous and Mesoporous Materials*, 295 (October 2019), 109961. DOI: 10.1016/j.micromeso.2019.109961.

[42] Tanjung, M.F., Zulys, A., Krisnandi, Y.K. (2025). Step-wise conversion of glucose into 2,5 furandicarboxylic acid (FDCA) in GVL-H2O solvent using hierarchical NiO/ZSM-5 catalyst. *Molecular Catalysis*, 586 (July), 115403. DOI: 10.1016/j.mcat.2025.115403.

[43] Guan, X., Duan, C., Wang, H., Lu, B., Zhao, J., Cai, Q. (2021). Tuneable oxidation of styrene to benzaldehyde and benzoic acid over Co/ZSM-5. *New J. Chem.*, 45(38), 18192–18201. DOI: 10.1039/D1NJ03145G.

[44] Kucherov, F.A., Romashov, L. V, Galkin, K.I., Ananikov, V.P. (2018). Chemical Transformations of Biomass-Derived C6-Furanic Platform Chemicals for Sustainable Energy Research, Materials Science, and Synthetic Building Blocks. *ACS Sustainable Chemistry & Engineering*, 6(7), 8064–8092. DOI: 10.1021/acssuschemeng.8b00971.

[45] Poliakoff, M., Licence, P., George, M.W. (2018). UN sustainable development goals: How can sustainable/green chemistry contribute? By doing things differently. *Current Opinion in Green and Sustainable Chemistry*, 13, 146–149. DOI: 10.1016/j.cogsc.2018.04.011.

[46] Liu, C., Wang, H., Karim, A.M., Sun, J., Wang, Y. (2014). Catalytic fast pyrolysis of lignocellulosic biomass. *Chemical Society Reviews*, 43(22), 7594–7623. DOI: 10.1039/c3cs60414d.

[47] Zhou, N., Thilakarathna, W.P.D.W., He, Q.S., Rupasinghe, H.P.V. (2022). A Review: Depolymerization of Lignin to Generate High-Value Bio-Products: Opportunities, Challenges, and Prospects. *Frontiers in Energy Research*, 9 (January), 1–18. DOI: 10.3389/fenrg.2021.758744.

[48] Rana, M., Ghosh, S., Nshizirungu, T., Park, J.H. (2023). Catalytic depolymerization of Kraft lignin to high yield alkylated-phenols over CoMo/SBA-15 catalyst in supercritical ethanol. *RSC Advances*, 13(43), 30022–30039. DOI: 10.1039/d3ra05018a.

[49] Sun, H., Luo, Z., Wang, W., Li, S., Xue, S. (2021). Porosity roles of micro-mesostructured ZSM-5 in catalytic fast pyrolysis of cellulolytic enzyme lignin for aromatics. *Energy Conversion and Management*, 247 (July), 114753. DOI: 10.1016/j.enconman.2021.114753.

[50] Lazaridis, P.A., Fotopoulos, A.P., Karakoulia, S.A. (2018). Catalytic Fast Pyrolysis of Kraft Lignin With Conventional , Mesoporous and Nanosized ZSM-5 Zeolite for the Production of Alkyl-Phenols and Aromatics. *Front. Chem.*, Sec. Green and Sustainable Chemistry, 6 (July). DOI: 10.3389/fchem.2018.00295.

[51] Kumar, C.R., Anand, N., Kloekhorst, A., Cannilla, C., Bonura, G., Frusteri, F., Barta, K., Heeres, H.J. (2015). Solvent free depolymerization of Kraft lignin to alkylphenolics using supported NiMo and CoMo catalysts. *Green Chemistry*, 17(11), 4921–4930. DOI: 10.1039/c5gc01641j.

[52] Guo, H., Zhao, Y., Chang, J.S., Lee, D.J. (2023). Lignin to value-added products: Research updates and prospects. *Bioresource Technology*, 384 (June), 129294. DOI: 10.1016/j.biortech.2023.129294.

[53] García-Rollán, M., Rivas-Márquez, M.N., Bertran-Llorens, S., Deuss, P.J., Ruiz-Rosas, R., Rosas, J.M., Rodríguez-Mirasol, J., Cordero, T. (2024). Biobased Vanillin Production by Oxidative Depolymerization of Kraft Lignin on a Nitrogen- and Phosphorus-Functionalized Activated Carbon Catalyst. *Energy and Fuels*, 38(8), 7018–7032. DOI: 10.1021/acs.energyfuels.4c00108.

[54] Hernández-Giménez, A.M., Heracleous, E., Pachatouridou, E., Horvat, A., Hernando, H., Serrano, D.P., Lappas, A.A., Bruijnincx, P.C.A., Weckhuysen, B.M. (2021). Effect of Mesoporosity, Acidity and Crystal Size of Zeolite ZSM-5 on Catalytic Performance during the Ex-situ Catalytic Fast Pyrolysis of Biomass. *ChemCatChem*, 13(4), 1207–1219. DOI: 10.1002/cctc.202001778.

[55] Ding, Y.L., Wang, H.Q., Xiang, M., Yu, P., Li, R.Q., Ke, Q.P. (2020). The Effect of Ni-ZSM-5 Catalysts on Catalytic Pyrolysis and Hydro-Pyrolysis of Biomass. *Frontiers in Chemistry*, 8 (September), 1–11. DOI: 10.3389/fchem.2020.00790.

[56] Shu, R., Lin, Y., Zhou, L., Luo, B., Yang, S., Tian, Z., Wang, C., Shi, Z., Nayak, R.R., Gupta, N.K. (2024). Enhanced lignin hydrogenolysis through synergy-induced bimetallic NiCu catalyst for chemocatalytic production of aromatic monomers. *Chemical Engineering Science*, 286 (November 2023), 119654. DOI: 10.1016/j.ces.2023.119654.

[57] Phillips, E.V., Tricker, A.W., Stavitski, E., Hatzell, M., Sievers, C. (2024). Mechanocatalytic Hydrogenolysis of the Lignin Model Dimer Benzyl Phenyl Ether over Supported Palladium Catalysts. *ACS Sustainable Chemistry and Engineering*, 12(33), 12306–12312. DOI: 10.1021/acssuschemeng.4c03590.

[58] Han, Y., Simmons, B.A., Singh, S. (2023). Perspective on oligomeric products from lignin depolymerization: their generation, identification, and further valorization. *Industrial Chemistry & Materials*, 1(2), 207–223. DOI: 10.1039/d2im00059h.

[59] Abolivier, R., Eckhardt, H.G., Sullivan, J.A. (2025). Study of Ni-ZSM-5 Catalysts in the Hydrogenolysis of Benzyl Phenyl Ether: Effects of Ni Loading, Morphology, and Reaction Conditions. *ACS Omega*, 10(12), 12306–12318. DOI: 10.1021/acsomega.4c11273.

[60] Li, J., Gao, M., Yan, W., Yu, J. (2022). Regulation of the Si/Al ratios and Al distributions of zeolites and their impact on properties. *Chemical Science*, 14(8), 1935–1959. DOI: 10.1039/d2sc06010h.

[61] Ávila, M.I., Alonso-Doncel, M.M., Cueto, J., Briones, L., Gómez-Pozuelo, G., Escola, J.M., Serrano, D.P., Peral, A., Botas, J.A. (2025). Production of high value-added phenolic compounds through lignin catalytic pyrolysis over ion-exchanged hierarchical ZSM-5 and Beta zeolites. *Catalysis Today*, 456 (March) DOI: 10.1016/j.cattod.2025.115343.

[62] Gao, Y., Zheng, B., Wu, G., Ma, F., Liu, C. (2016). Effect of the Si/Al ratio on the performance of hierarchical ZSM-5 zeolites for methanol aromatization. *RSC Advances*, 6(87), 83581–83588. DOI: 10.1039/c6ra17084f.

[63] Gou, J., Wang, Z., Li, C., Qi, X., Vattipalli, V., Cheng, Y.T., Huber, G., Conner, W.C., Dauenhauer, P.J., Mountziaris, T.J., Fan, W. (2017). The effects of ZSM-5 mesoporosity and morphology on the catalytic fast pyrolysis of furan. *Green Chemistry*, 19(15), 3549–3557. DOI: 10.1039/c7gc01395g.

[64] Toledano, A., Serrano, L., Pineda, A., Romero, A.A., Luque, R., Labidi, J. (2014). Microwave-assisted depolymerisation of organosolv lignin via mild hydrogen-free hydrogenolysis: Catalyst screening. *Applied Catalysis B: Environmenta*l, 145, 43–55. DOI: 10.1016/j.apcatb.2012.10.015.

[65] Tang, Y., Yang, X., Zhang, Q., Lv, D., Zuo, S., Li, J. (2025). Comprehensive Analysis of the Synergistic Effects of Bimetallic Oxides in CoM/γ-Al2O3 (M = Cu, Fe, or Ni) Catalysts for Enhancing Toluene Combustion Efficiency. *Molecules*, 30(5), 1–14. DOI: 10.3390/molecules30051188.